Applied Physics Letters

RESEARCH ARTICLE | SEPTEMBER 11 2023

Mass and shape determination of optically levitated nanoparticles

Bart Schellenberg ; Mina Morshed Behbahani ; Nithesh Balasubramanian ; Ties H. Fikkers ; Steven Hoekstra

Appl. Phys. Lett. 123, 114102 (2023)
https://doi.org/10.1063/5.0166136

AIP Publishing

Applied Physics Letters ARTICLE pubs.aip.org/aip/apl

Mass and shape determination of optically levitated nanoparticles

Cite as: Appl. Phys. Lett. **123**, 114102 (2023); doi: 10.1063/5.0166136
Submitted: 3 July 2023 · Accepted: 1 August 2023 ·
Published Online: 11 September 2023

Bart Schellenberg, Mina Morshed Behbahani, Nithesh Balasubramanian, Ties H. Fikkers, and Steven Hoekstra[a)]

AFFILIATIONS

Van Swinderen Institute, University of Groningen, The Netherlands and Nikhef, Amsterdam, The Netherlands

[a)]Author to whom correspondence should be addressed: s.hoekstra@rug.nl

ABSTRACT

When introducing a nanoparticle into an optical trap, its mass and shape are not immediately apparent. We combine a charge-based mass measurement with a shape determination method based on light scattering and an analysis of the damping rate anisotropy, all on the same set of silica nanoparticles, trapped using optical tweezers in vacuum. These methods have previously only been used separately, and the mass determination method has not been applied to asymmetric particles before. We demonstrate that the combination of these classification techniques is required to distinguish particles with similar mass but different shape, and vice versa. The ability to identify these parameters is a key step for a range of experiments on precision measurements and sensing using optically levitated nanoparticles.

With a rapidly increasing number of developments over the recent years, levitated nanospheres have evolved into an exciting platform for innovative measurement opportunities and applications. Demonstrated applications span from the manipulation of microscopic biological systems[1–4] to ultra-sensitive accelerometers and force-sensors,[5–9] torque detectors,[10–13] hyper-fast mechanical rotors,[14–16] and measurements on thermal diffusion.[17–21] Numerous proposals in recent years have explored the potential of using isolated nanometer-sized particles for probing gravitational waves,[22,23] to observe quantum gravity,[24–26] to employ in the dark matter scattering experiments,[27,28] or to trial quantum collapse models.[29] For numerous of these[8–13,27,28] and other[30–34] applications, knowing the precise mass and morphology of the levitated particles is essential. When introducing a particle into an optical tweezer, however, its shape and mass are not immediately apparent. Particles from a monodisperse solution of spheres have been observed to regularly carry some non-negligible ellipticity[35] or they may aggregate to form composite structures.[10]

While mass determination of charged particles and shape determination through the anisotropy of light scattering and the damping rate have been demonstrated on an individual basis, a comprehensive correlative study of these techniques applied to a set of differently shaped and sized particles remains unexplored. In this work, we present the shape and mass determination for optically levitated silica nanoparticles of various sizes and shapes in vacuum. We demonstrate that the combination of these classification techniques is required to discriminate between different particles. We manage to capture both single particles as well as aggregated structures in an optical tweezer trap by adjusting the concentration of a monodisperse solution of nanospheres.[10] As illustration of some of the typical shapes that we encounter, Fig. 1 shows a scanning electron microscope picture of our solution. To unambiguously determine the mass and shape of the optically levitated nanoparticles, we combine the above-mentioned *in situ* classification methods.

Specifically, we extend the mass determination that was previously demonstrated for nanospheres[36,37] to asymmetric compositions of nanospheres, using similar and smaller sizes. We combine this method with the shape determination from a non-isotropic damping rate due to residual background gas.[10,38] In addition, by employing a secondary probe laser, we find the particle's morphology through its angle-resolved Rayleigh scattering profile.[35] We discuss the reliability of each method individually as well as their combined results. Our approach does not rely on precise calculations of the moment of inertia or the polarizability of the particle.

The structure of this paper is as follows. Following an introduction of the experimental setup, we present the methods and results from each individual classification technique to determine the properties of a fixed set of particles. After that we correlate and discuss the combined results.

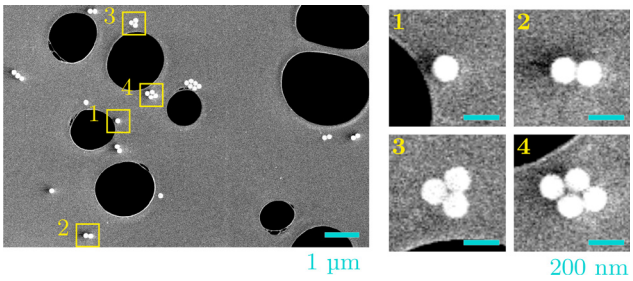

FIG. 1. Two pictures revealing possible shapes of the (composite) nanoparticles used for this paper, taken using a scanning electron microscope. The black patches represent holes in the holey carbon substrate. The left picture shows some of the nanoparticles used for trapping, where each sphere has a diameter of 142 ± 4 nm, according to the manufacturer. The panels on the right show a close-up of several composite structures.

We combine a number of standard techniques[39] to optically trap nanoparticles in a controlled pressure environment. A schematic of our experimental setup is shown in Fig. 2. We use the light of a Coherent Nd:YAG Mephisto MOPA trapping laser ($\lambda_{\text{trap}} = 1064$ nm) and a spatial filter (SF) to obtain a Gaussian trapping beam. Using a half-waveplate (HWP), we control its polarization. The light then enters the vacuum chamber through a window and is focused using a microscope objective (MO; NA = 0.8), establishing the dipole trap at its focus point. The strong and inhomogeneous electric field at the focus creates a gradient force on the dielectric nanoparticles, allowing them to be trapped at the focus. We evaporate silica (SiO_2) nanospheres (diameters 103 ± 6, 142 ± 4 nm; Microparticles GmbH) from an ethanol solution using a medical nebuliser[40] at ambient pressure near the trapping region. When a droplet from the cloud of ethanol, carrying a nanoparticle, passes through the optical trap, the particle can be caught. Once the particle is trapped, we reduce the pressure toward the operational domain between ∼20 and ∼0.1 mbar.

Surrounding the trapping region, we have placed two copper electrodes (CE), with which we create a controlled electric field at the location of the trapped particle. We placed a discharge electrode (QE) to be able to charge/discharge the trapped nanoparticle.[36,37] The electrode setup is used in the mass measurement of the nanoparticle. To visualize the trapped nanoparticle and to measure its angular Rayleigh scattering profile, we use the light of a probe diode laser

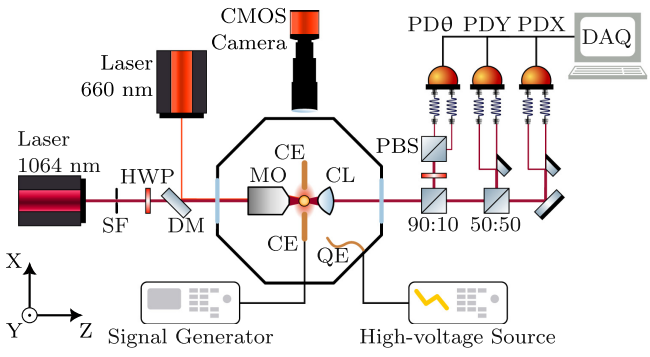

FIG. 2. A schematic representation of the experimental setup. Details are presented in the main text.

($\lambda_{\text{probe}} = 660$ nm) and overlap this beam with the trapping beam using a dichroic mirror (DM). A fraction of the scattered light at λ_{probe} is collected using a CMOS camera. To track the dynamics of the particle inside the trap, we collect the transmitted trapping light using a collection lens (CL) and guide it toward a series of beamsplitters. We first use 10% of the remaining light for the angular detection, by employing a polarizing beam splitter (PBS) and a differential photodiode (PD θ), which is balanced by another HWP. The final 90% is used for the X and Y detection, which include a D-shaped mirror and a differential photodiode (PDX and PDY), to measure the spatial intensity differences within the beam profile.

For each particle whose data are represented in this paper, the same experimental procedure was conducted. A detailed description on this procedure is given in Appendix A of the supplementary material. The particle is essentially cleaned from possible residual water in the porous internal silica structure[37,41,42] and charged to about 6–10 charges in preparation of the mass measurement. Once ready, we perform the mass measurements and record the angular Rayleigh scattering profile in the harmonic regime at around 20 mbar. We then periodically record the particle's signal during a slow pump-down, to determine its damping rate as a function of pressure.

When the translational damping of the particle is sufficiently high ($\gtrsim$3 mbar), its motion is primarily described by the (single-sided) linear power spectral density (PSD)[43,44]

$$S_F(\Omega) = \frac{k_B T}{m} \frac{\Gamma_0}{(\Omega_0^2 - \Omega^2)^2 + \Omega^2 \Gamma_0^2}, \tag{1}$$

which can be directly obtained from the signals recorded by PDX and PDY. Here, Ω_0 represents the natural oscillation frequency and Γ_0 is the damping rate of the nanoparticle due to the background gas, both in rad/s. The mass of the particle is denoted with m, and k_B and T are the Boltzmann constant and the heatbath temperature, respectively. The subscript F is used to denote that Eq. (1) is driven by the thermal fluctuation force. Figure 3(a) shows a typical translational PSD from a spherical nanoparticle. The cyclic frequencies of the X and Y channels are not degenerate due to some ellipticity in the optical trap.[45] We obtain the natural frequency Ω_0 and the damping rates Γ_0 by fitting Eq. (1) to Fig. 3(a). To obtain an impression of the ellipticity of the particle's morphology, we also use the torsional PSD, recorded by PD θ. Typical torsional PSDs for three different particles are shown in Fig. 3(b). The three particles were classified as a nanosphere, a dumbbell, and a triangle trimer, using the techniques described in this paper. We observe similar trap frequencies Ω_0 (and, therefore, similar trap stiffness) for the translational motion of these three particles.

In linearly polarized light, the asymmetric susceptibility tensor of a non-spherical particle will introduce a torque to the system that causes the particle to align its major axis of polarizability with the polarization of the trapping light. One of the consequences of this laser-induced alignment is that the measured damping rates in the X and Y channels become unequal. This anisotropy in the damping rates can be used as a measure of the asymmetry of the particle's shape.[10,38] Figure 4(a) shows the damping rates of a nanoparticle, which was classified as a dumbbell, as a function of the pressure. Figure 4(b) shows the corresponding ratio $\Gamma_0^{(y)}/\Gamma_0^{(x)}$, as well as that of a sphere and a triangle trimer. The nanodumbbell shows a high degree of asymmetry, with a ratio $\Gamma_0^{(y)}/\Gamma_0^{(x)} \approx 1.27$, which is in agreement with that of a dumbbell with a length-to-diameter ratio close to 1.7 (Ref. 10).

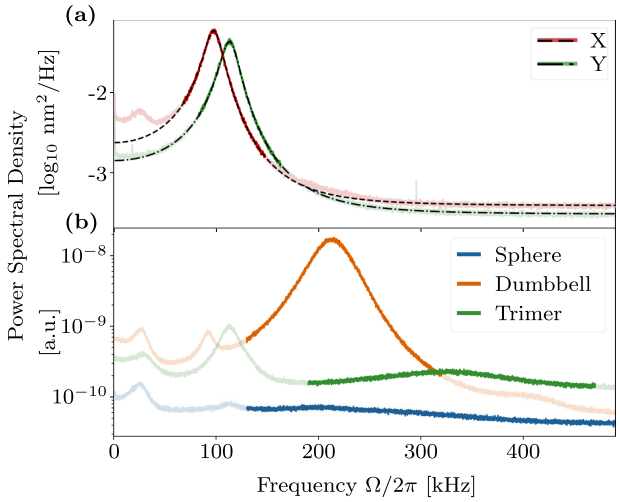

FIG. 3. Typical power spectral densities (PSD) of the trapped nanoparticles. (a) The transverse (X,Y) motion of a spherical nanoparticle (particle 15 from Fig. 7). The dashed/dotted lines indicate the best-fit of Eq. (1); (b) PSDs of the signal recorded by PD θ for three particles (15, 18, and 6 from Fig. 7); The additional peaks in both insets correspond to the Z, X, and Y motions of the particle. (See Appendix C of the supplementary material for further details.) The highlighted parts in both insets indicate the regions where the signal of interest dominates, which are used for the analysis.

Meanwhile, the sphere ($\Gamma_0^{(y)}/\Gamma_0^{(x)} \approx 1.03$) and trimer ($\Gamma_0^{(y)}/\Gamma_0^{(x)} \approx 1.11$) appear to be much more symmetric in the XY plane of the setup, as is in agreement with simulated results,[38] and they require additional classification techniques to be unambiguously distinguished from one another.

In addition to the asymmetric damping rates, we also record the angle-resolved Rayleigh scattering profile of the particle, which was recently demonstrated to allow the detection of asymmetries in the particle's morphology down to a few nanometers[35] in the XY-plane of our setup. To realize this procedure, we use the probe laser (co-propagating with the trapping laser along the Z axis) to illuminate the nanoparticle inside the optical trap at a different wavelength ($\lambda_{\text{probe}} = 660\,\text{nm}$) and lower power ($\sim$2 mW) from the trapping laser ($\lambda_{\text{trap}} = 1064\,\text{nm}$; $\sim$330 mW). A HWP is used to rotate the linear polarization of the trapping laser, while keeping that of the probe laser fixed. The laser induced optical alignment of an asymmetric particle then allows us to effectively rotate it about the longitudinal Z axis of our setup. The scattered light is then detected at a right angle using a 12-bit CMOS camera, from which we track the averaged intensity over a closed pixel region around the particle. To improve the signal-to-noise ratio, we image the nanoparticle slightly out of focus, such that we could adjust the gain of the camera without causing the pixels to immediately saturate. A dichroic mirror is used to prevent the scattered light at the trapping wavelength from reaching the camera.

Theoretically, the expected scattering intensity can be obtained from the particle's susceptibility tensor as follows:[35]

$$I(\theta) \propto \left(\chi^{(yy)}\right)^2; \text{ with } \boldsymbol{\chi}(\theta) = \boldsymbol{R}\boldsymbol{\chi}_0\boldsymbol{R}^\top, \tag{2}$$

where $\boldsymbol{\chi}_0$ represents the susceptibility tensor in the particle's eigenframe, and $\boldsymbol{R}$ is the rotation matrix to map to the laboratory frame. For the case of a dumbbell specifically, values for $\chi_0^{(yy)}/\chi_0^{(xx)}$ have been computed[10] and suggest $I_{\text{min}}/I_{\text{max}} \approx 0.75$ when the length to diameter ratio reaches close to 1.7. Figure 5 shows the resulting data for three particles, which were classified as a nanosphere, a dumbbell, and a triangle trimer. The susceptibility tensor of the particle in Fig. 5(a) appears to be almost fully symmetrical in the XY-plane, however, the data reveal some small ellipticity of the particle at $I_{\text{min}}/I_{\text{max}} \approx 0.99$. In contrast, the particle in Fig. 5(b) shows a high degree of asymmetry between $\chi_0^{(yy)}$ and $\chi_0^{(xx)}$, with $I_{\text{min}}/I_{\text{max}} \approx 0.72$, and most likely resulted from a dumbbell. The particle in Fig. 5(c), however, shows far less contrast and could not be distinguished from a single elliptical nanosphere based on the scattering data alone. By including its mass and damping rate measurements, this particle was classified as a triangle trimer.

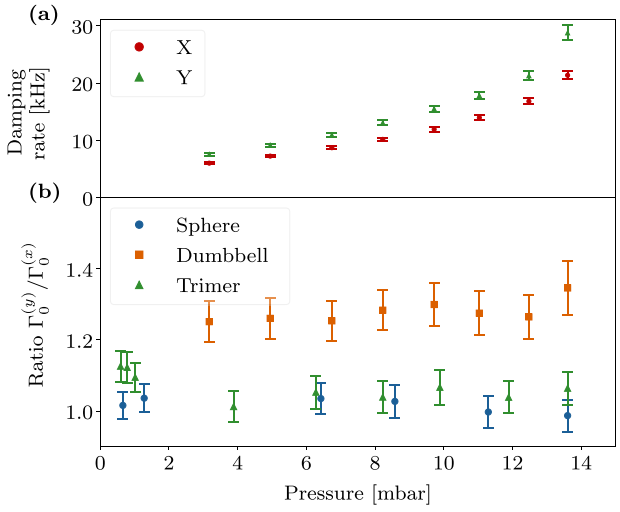

FIG. 4. (a) The damping rate of a nanoparticle as a function of pressure, corresponding to particle 3 from Fig. 7; (b) the ratio $\Gamma_0^{(y)}/\Gamma_0^{(x)}$ for a set of different particles, which were classified as a sphere, a dumbbell, and a triangle trimer. The particles correspond to 15, 3, and 6 from Fig. 7, respectively.

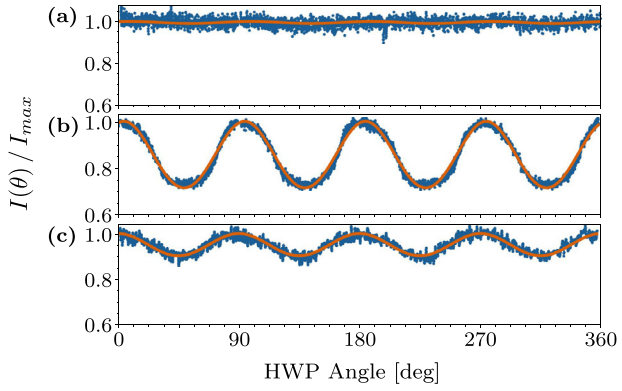

FIG. 5. Measured Rayleigh scattering profile for several different particles. Each particle shown in this figure consisted of a number of nanospheres, with an individual size of $d = 103 \pm 6\,\text{nm}$. The data were taken from particles 1, 3, and 6 from Fig. 7, respectively.

The instantaneous inertial response of the nanoparticle to a well-defined externally applied force may be used to directly determine the mass of the particle. A protocol for the active control over the nanoparticle's electric charge has already been developed[37] and is also elaborated on in Appendix A of the supplementary material. We use the CE to harmonically drive the charged particle using a quasi-static electric field near its natural oscillation frequency. Due to the zero correlation between the electrical driving force and the random Brownian fluctuation force, which is responsible for Eq. (1), the PSD of this driven system can be written by simply appending the additional term[36]

$$S_M(\Omega) = \frac{F_0^2\tau}{8m^2}\frac{\mathrm{sinc}\left(\frac{1}{2}(\Omega-\Omega_M)\tau\right)}{(\Omega_0^2-\Omega^2)^2+\Omega^2\Gamma_0^2} \tag{3}$$

to Eq. (1). In this new term, F_0 represents the amplitude of the applied sinusoidal force, Ω_M is the frequency of this force, and τ is the duration of the finitely recorded signal used to compute the Fourier transform. The subscript M is used to denote that Eq. (3) results from the modulation force that is applied to the particle. While Eq. (1) scales with the inverse of the particle's mass m, Eq. (3) does with its square. Therefore, the ratio,

$$\frac{S_F(\Omega_M)}{S_M(\Omega_M)} = \frac{8\Gamma_0 k_B T}{F_0^2\tau}m, \tag{4}$$

may be used to extract the particle's mass.

Figures 6(a) and 6(b) show two examples of the PSD following two harmonically driven nanoparticles, which were classified as a sphere and a dumbbell. The inset in both figures shows a close-up of the PSD around the driving frequency Ω_M, revealing the sinc-shape as described by Eq. (3). The dashed lines on both show the corresponding fits to Eq. (1) for the large-scale figure and Eq. (3) for the inset. Both particles are driven using the exact same force, and the presented data were recorded at the same pressure (∼15 mbar). Nonetheless, it can be seen that Fig. 6(b) has a lower peak and a smaller overall width than Fig. 6(a), the latter of which relates to a lower damping rate Γ_0. Both properties indicate that Fig. 6(b) was taken from a heavier particle than Fig. 6(a). Below, in Fig. 6(c), the resulting mass is shown for both particles in femtograms. To improve our statistics, we measure each particle for a series of driving frequencies Ω_M around the particle's natural frequency Ω_0. From the results, it can be seen that the mass of the dumbbell is about twice as much as that of a single sphere.

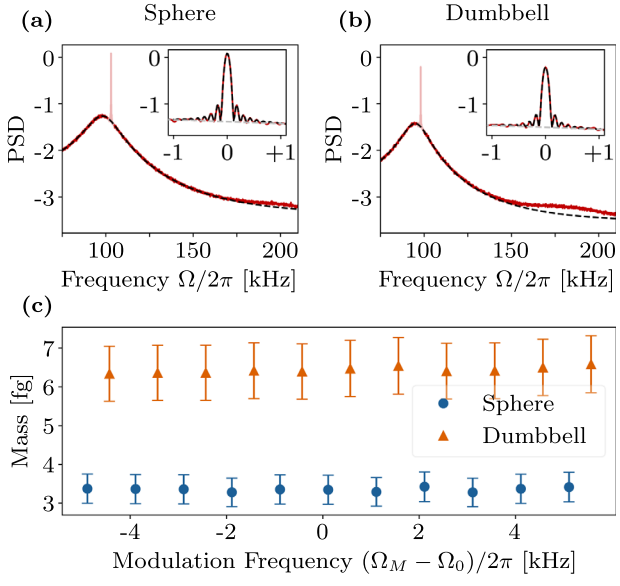

FIG. 6. Mass data for two particles. (a) and (b) show the PSDs following two harmonically driven particles, alongside an enlarged version of the driving peak in the inset, following Eq. (3). The dashed lines in both figures represent the best-fit to Eqs. (1) and (3). In (b), one may observe that part of the torsional signal is leaked into the data starting around 180 kHz. (a) and (b) correspond to particles 15 and 17 in Fig. 7. (c) shows the resulting mass measurements for both particles, measured for a series of driving frequencies Ω_M around the natural frequency Ω_0.

We will now consider the combined results of the damping rate, scattering, and mass measurements. Figure 7 shows an overview of a set of 18 different nanoparticles. For each particles, we have performed the three classification methods, which leads us to categorize as indicated at the bottom of the figure. The horizontal dashed lines represent the average results and the standard deviation of the spread, for each classification category.

As a single classification technique, the mass measurements appear to show the best resolution. We classify particles whose masses are approximately twice as much as that of the corresponding spheres

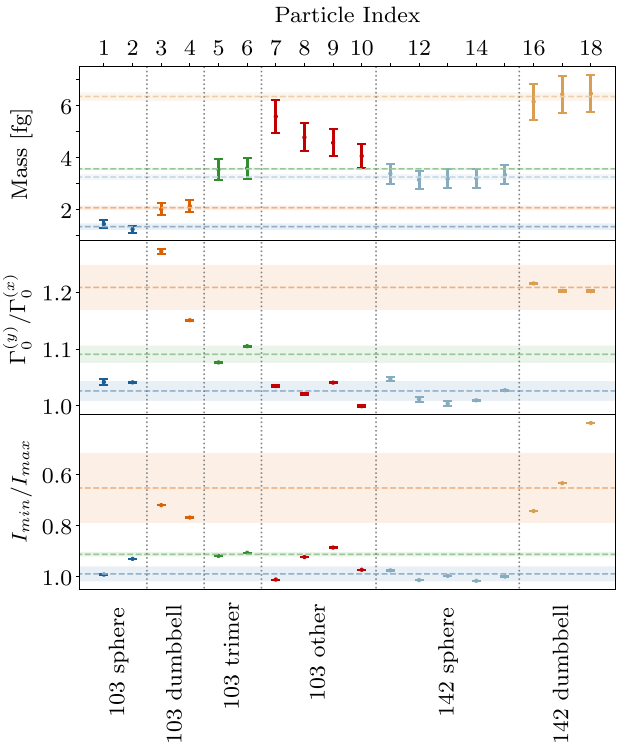

FIG. 7. The combined results from the mass, damping rate, and scattering measurements, sorted by their classified categories. The data on each column correspond to the same particles. The horizontal dashed lines represent the average result per category (excluding other, which represents compositions of four or more spheres), and the colored band shows the standard deviation of the data points.

as dumbbells and those which are three times as much as trimers. We find that the mass of a nanoparticle is typically a bit high compared to the specifications of the manufacturer. One likely reason for this is the presence of residual water in the silica structure.[37,41,42] However, also uncertainties in the mass density of the nanoparticles play a role.[37,42] (See also Appendix A in the supplementary material for more details.) Our results on the mass determination are in line with those obtained in other publications.[36,37]

The measurements on the scattering profile and the damping rates do not show a significant difference between the nanoparticles composed of 103 or 142 nm spheres, as these methods focus on the morphology of the particle. Neither does either of the methods single-handedly give a satisfactory resolution that allows for an unambiguous distinction between single spheres, triangle trimers, and particles composed of four or more nanospheres (denoted as "other" in Fig. 7). In this case, the combination of multiple classification techniques is required to classify the particle.

On a single particle level, the measurements on the mass and shape using the three methods (PSD analysis, scattering anisotropy, and mass determination) are reproducible and show consistent results. When comparing multiple particles of the same category with each other, however, we see significant scattering of the data beyond the statistical error bars, which lead us to perform an analysis of the main systematic effects that influence these measurements. Here, we present the main conclusions, while the full details are given in the supplementary material.

Concerning the mass measurement, the accuracy with which we can determine the distance between the copper electrodes limits the accuracy with which we can quantify the mass of the particle. In our results, this is given as a symmetric uncertainty of 5.6% in the value of the electric field. The fitting of the PSD, which is used to assess the morphology of the particle, is influenced by the crosstalk between the different motional modes of the particle. At pressure below a few mbar, where damping by background gas is reduced, the anharmonic part of the potential is explored, which leads to a reduced quality of the fits. We find an overestimation of the damping rate of a given motional degree of freedom in the pressure range we use by at most 5%. Regarding the scattering anisotropy, we have evaluated detector linearity and alignment as potential systematic effects, which play a minor role. In this paper, we have primarily demonstrated the classification of spheres, dumbbells, and triangle trimers, as these appear to be some of the simplest configurations that we most often trap from our solutions. However, nanospheres can also aggregate into different shapes, such as chain trimers, or obtuse configurations. These shapes were not observed in our measurements, which we suspect is due to the stability of our trap and the rate at which these configurations form in our solution.

We have combined a charge-based mass measurement with a shape determination method based on light-scattering and an analysis of the damping rate anisotropy, all on the same set of trapped nanoparticles. We observe a large variation in the shapes and sizes within a set of nanoparticles. This is not only caused by the variation in the shape and mass of the individual spheres but also by the way in which they combine to form composite particles. We have demonstrated that the combination of these classification techniques enables us to obtain an unambiguous conclusion on the particle's shape, size, and mass.

See the supplementary material for a detailed description of the measurement protocol, the data analysis (specifically for obtaining the damping rate Γ_0), and the consideration of systematic effects in all three classification techniques.

We acknowledge the support from Gert ten Brink, Leo Huisman, and George Palasantzas. This project has received funding from NWO through NWA Startimpuls (No. 400.17.608/4303).

AUTHOR DECLARATIONS

Conflict of Interest

The authors have no conflicts to disclose.

Author Contributions

Bart Schellenberg: Conceptualization (equal); Data curation (equal); Formal analysis (lead); Investigation (equal); Methodology (equal); Software (equal); Validation (equal); Visualization (equal); Writing – original draft (equal); Writing – review & editing (equal). **Mina Morshed Behbahani:** Conceptualization (equal); Data curation (equal); Investigation (equal); Methodology (equal); Software (equal); Validation (equal); Visualization (equal); Writing – original draft (equal); Writing – review & editing (equal). **Nithesh Balasubramanian:** Conceptualization (equal); Formal analysis (supporting); Investigation (equal); Methodology (equal); Software (equal); Writing – original draft (supporting); Writing – review & editing (equal). **Ties Hendrik Fikkers:** Conceptualization (equal); Investigation (equal); Methodology (equal); Writing – original draft (supporting); Writing – review & editing (equal). **Steven Hoekstra:** Conceptualization (equal); Funding acquisition (lead); Investigation (equal); Methodology (equal); Validation (equal); Visualization (equal); Writing – original draft (equal); Writing – review & editing (equal).

DATA AVAILABILITY

The data that support the findings of this study are available from the corresponding author upon reasonable request.

REFERENCES

[1]I. Heller, T. P. Hoekstra, G. A. King, E. J. G. Peterman, and G. J. L. Wuite, "Optical tweezers analysis of DNA–protein complexes," Chem. Rev. **114**, 3087–3119 (2014).
[2]P. Mangeol, D. Côte, T. Bizebard, O. Legrand, and U. Bockelmann, "Probing DNA and RNA single molecules with a double optical tweezer," Eur. Phys. J. E **19**, 311–317 (2006).
[3]M. Wang, H. Yin, R. Landick, J. Gelles, and S. Block, "Stretching DNA with optical tweezers," Biophysical J. **72**, 1335–1346 (1997).
[4]C. Arbore, L. Perego, M. Sergides, and M. Capitanio, "Probing force in living cells with optical tweezers: From single-molecule mechanics to cell mechanotransduction," Biophys. Rev. **11**, 765–782 (2019).
[5]J. Gieseler, L. Novotny, and R. Quidant, "Thermal nonlinearities in a nanomechanical oscillator," Nat. Phys. **9**, 806–810 (2013).
[6]D. Hempston, J. Vovrosh, M. Toroš, G. Winstone, M. Rashid, and H. Ulbricht, "Force sensing with an optically levitated charged nanoparticle," Appl. Phys. Lett. **111**, 133111 (2017).
[7]C. W. Lewandowski, T. D. Knowles, Z. B. Etienne, and B. D'Urso, "High-sensitivity accelerometry with a feedback-cooled magnetically levitated microsphere," Phys. Rev. Appl. **15**, 014050 (2021).
[8]G. Ranjit, M. Cunningham, K. Casey, and A. A. Geraci, "Zeptonewton force sensing with nanospheres in an optical lattice," Phys. Rev. A **93**, 053801 (2016).

[9]E. Hebestreit, M. Frimmer, R. Reimann, and L. Novotny, "Sensing static forces with free-falling nanoparticles," Phys. Rev. Lett. **121**, 063602 (2018).
[10]J. Ahn, Z. Xu, J. Bang, Y.-H. Deng, T. M. Hoang, Q. Han, R.-M. Ma, and T. Li, "Optically levitated nanodumbbell torsion balance and GHz nanomechanical rotor," Phys. Rev. Lett. **121**, 033603 (2018).
[11]J. Ahn, Z. Xu, J. Bang, P. Ju, X. Gao, and T. Li, "Ultrasensitive torque detection with an optically levitated nanorotor," Nat. Nanotechnol. **15**, 89–93 (2020).
[12]A. L. Porta and M. D. Wang, "Optical torque wrench: Angular trapping, rotation, and torque detection of quartz microparticles," Phys. Rev. Lett. **92**, 190801 (2004).
[13]G. D. Bruce, P. Rodríguez-Sevilla, and K. Dholakia, "Initiating revolutions for optical manipulation: The origins and applications of rotational dynamics of trapped particles," Adv. Phys.: X **6**, 1838322 (2020).
[14]Y. Arita, M. Mazilu, and K. Dholakia, "Laser-induced rotation and cooling of a trapped microgyroscope in vacuum," Nat. Commun. **4**, 2374 (2013).
[15]R. Reimann, M. Doderer, E. Hebestreit, R. Diehl, M. Frimmer, D. Windey, F. Tebbenjohanns, and L. Novotny, "GHz rotation of an optically trapped nanoparticle in vacuum," Phys. Rev. Lett. **121**, 033602 (2018).
[16]Y. Jin, J. Yan, S. J. Rahman, J. Li, X. Yu, and J. Zhang, "6 GHz hyperfast rotation of an optically levitated nanoparticle in vacuum," Photonics Res. **9**, 1344 (2021).
[17]T. Li, S. Kheifets, D. Medellin, and M. G. Raizen, "Measurement of the instantaneous velocity of a Brownian particle," Science **328**, 1673–1675 (2010).
[18]L. Bellando, M. Kleine, Y. Amarouchene, M. Perrin, and Y. Louyer, "Giant diffusion of nanomechanical rotors in a tilted washboard potential," Phys. Rev. Lett. **129**, 023602 (2022).
[19]J. Gieseler and J. Millen, "Levitated nanoparticles for microscopic thermodynamics—A review," Entropy **20**, 326 (2018).
[20]T. M. Hoang, R. Pan, J. Ahn, J. Bang, H. T. Quan, and T. Li, "Experimental test of the differential fluctuation theorem and a generalized Jarzynski equality for arbitrary initial states," Phys. Rev. Lett. **120**, 080602 (2018).
[21]T. Li and M. G. Raizen, "Brownian motion at short time scales," Ann. Phys. **525**, 281–295 (2013).
[22]A. Arvanitaki and A. A. Geraci, "Detecting high-frequency gravitational waves with optically levitated sensors," Phys. Rev. Lett. **110**, 071105 (2013).
[23]R. J. Marshman, A. Mazumdar, G. W. Morley, P. F. Barker, S. Hoekstra, and S. Bose, "Mesoscopic interference for metric and curvature & gravitational wave detection," New J. Phys. **22**, 083012 (2020).
[24]Y. Margalit, O. Dobkowski, Z. Zhou, O. Amit, Y. Japha, S. Moukouri, D. Rohrlich, A. Mazumdar, S. Bose, C. Henkel, and R. Folman, "Realization of a complete Stern-Gerlach interferometer: Toward a test of quantum gravity," Sci. Adv. **7**, eabg2879 (2021).
[25]T. W. V. D. Kamp, R. J. Marshman, S. Bose, and A. Mazumdar, "Quantum gravity witness via entanglement of masses: Casimir screening," Phys. Rev. A **102**, 062807 (2020).
[26]C. Marletto and V. Vedral, "Gravitationally induced entanglement between two massive particles is sufficient evidence of quantum effects in gravity," Phys. Rev. Lett. **119**, 240402 (2017).
[27]G. Afek, D. Carney, and D. C. Moore, "Coherent scattering of low mass dark matter from optically trapped sensors," Phys. Rev. Lett. **128**, 101301 (2022).
[28]F. Monteiro, G. Afek, D. Carney, G. Krnjaic, J. Wang, and D. C. Moore, "Search for composite dark matter with optically levitated sensors," Phys. Rev. Lett. **125**, 181102 (2020).
[29]A. Vinante, A. Pontin, M. Rashid, M. Toroš, P. F. Barker, and H. Ulbricht, "Testing collapse models with levitated nanoparticles: Detection challenge," Phys. Rev. A **100**, 012119 (2019).
[30]C. Gonzalez-Ballestero, M. Aspelmeyer, L. Novotny, R. Quidant, and O. Romero-Isart, "Levitodynamics: Levitation and control of microscopic objects in vacuum," Science **374**, eabg3027 (2021).
[31]B. A. Stickler, K. Hornberger, and M. S. Kim, "Quantum rotations of nanoparticles," Nat. Rev. Phys. **3**, 589 (2021).
[32]T. K. Sau and A. L. Rogach, "Nonspherical noble metal nanoparticles: Colloid–chemical synthesis and morphology control," Adv. Mater. **22**, 1781–1804 (2010).
[33]A. Sirelkhatim, S. Mahmud, A. Seeni, N. H. M. Kaus, L. C. Ann, S. K. M. Bakhori, H. Hasan, and D. Mohamad, "Review on zinc oxide nanoparticles: Antibacterial activity and toxicity mechanism," Nano-Micro Lett. **7**, 219–242 (2015).
[34]X. Huang and M. A. El-Sayed, "Gold nanoparticles: Optical properties and implementations in cancer diagnosis and photothermal therapy," J. Adv. Res. **1**, 13–28 (2010).
[35]M. Rademacher, J. Gosling, A. Pontin, M. Toroš, J. T. Mulder, A. J. Houtepen, and P. F. Barker, "Measurement of single nanoparticle anisotropy by laser induced optical alignment and Rayleigh scattering for determining particle morphology," Appl. Phys. Lett. **121**, 221102 (2022).
[36]F. Ricci, M. T. Cuairan, G. P. Conangla, A. W. Schell, and R. Quidant, "Accurate Mass Measurement of a Levitated Nanomechanical Resonator for Precision Force-Sensing," Nano Lett. **19**, 6711–6715 (2019).
[37]F. Ricci, "Levitodynamics toward force nano-sensors in vacuum," Ph.D. thesis (Universitat Politècnica de Catalunya, 2019).
[38]J. Ahn, "Spin optomechanics of levitated nanoparticles," Ph.D. thesis (Purdue University, 2020).
[39]J. Gieseler, B. Deutsch, R. Quidant, and L. Novotny, "Subkelvin parametric feedback cooling of a laser-trapped nanoparticle," Phys. Rev. Lett. **109**, 103603 (2012).
[40]M. D. Summers, D. R. Burnham, and D. McGloin, "Trapping solid aerosols with optical tweezers: A comparison between gas and liquid phase optical traps," Opt. Express **16**, 7739 (2008).
[41]L. Zhuravlev, "The surface chemistry of amorphous silica. Zhuravlev model," Colloids Surf., A **173**, 1–38 (2000).
[42]S. R. Parnell, A. L. Washington, A. J. Parnell, A. Walsh, R. M. Dalgliesh, F. Li, W. A. Hamilton, S. Prevost, J. P. A. Fairclough, and R. Pynn, "Porosity of silica Stöber particles determined by spin-echo small angle neutron scattering," Soft Matter **12**, 4709–4714 (2016).
[43]J. Gieseler, "Dynamics of optically levitated nanoparticles in high vacuum," Ph.D. thesis (ICFO, 2014).
[44]E. Hebestreit, "Thermal properties of levitated nanoparticles," Ph.D. thesis (ETH Zürich, 2017).
[45]Y. Jin, X. Yu, and J. Zhang, "Polarization-dependent center-of-mass motion of an optically levitated nanosphere," J. Opt. Soc. Am. B **36**, 2369 (2019).